

## Neutron scattering cross sections for $^{204,206}\text{Pb}$ and neutron and proton amplitudes of $E2$ and $E3$ excitations

Sally F. Hicks

*Department of Physics, University of Dallas, Irving, Texas 75062*

J. M. Hanly,\* S. E. Hicks,<sup>†</sup> G. R. Shen,<sup>‡</sup> and M. T. McEllistrem

*Department of Physics and Astronomy, University of Kentucky, Lexington, Kentucky 40506*

(Received 6 August 1993)

Differential elastic and inelastic scattering cross sections have been measured for neutrons incident on  $^{204}\text{Pb}$  and  $^{206}\text{Pb}$  at energies of 2.5, 4.6, and 8.0 MeV and total cross sections in 100-keV steps from 250 keV to 4.0 MeV. Both spherical and coupled-channels analyses have been used to interpret this large set of data, together with other total cross sections extending to 8 MeV. Several purposes motivate this work. The first is to establish the dispersion-corrected mean field appropriate for these nuclei. A consistent description of the energy dependent neutron scattering potential includes a dispersion relation connecting the real and imaginary parts of the potential; the resultant potential relates the energy dependent scattering field to one representing bound single particle levels. Dispersion relations using both the single channel and coupled-channels models have been examined; both give very similar results. The second motivation is to deduce neutron and proton excitation strengths of the lowest-energy quadrupole and octupole excitations seen via neutron scattering, and to compare those strengths with similar values derived from electromagnetic excitation, heavy-ion and pion scattering. The role of target neutrons in both collective excitations was found to be enhanced compared to the proton role.

PACS number(s): 25.40.Dn, 25.40.Fq, 27.80.+w, 28.20.Cz

### I. INTRODUCTION

Neutron excitation amplitudes for low-lying collective levels in the highly collective nuclei near  $A = 190$  are very different than proton scattering or electromagnetic excitation amplitudes [1-4]. This is in contrast to what had been expected [5,6] and found for deformed nuclei [5,7]. Neutron-proton symmetry is substantially broken for the shape-transitional nuclei near  $A = 190$ . Moreover these departures from neutron-proton symmetry in collective excitations are quite different for the Pt nuclei, where the ground band is affected, than for the Os nuclei [3,4,2] where it is the quasigamma band that is most severely affected.

Most of the cases of non-isoscalar collective excitations are small departures from symmetry [8] of electric quadrupole ( $E2$ ) character. A very recent survey of both  $E2$  and electric octupole ( $E3$ ) levels in nuclei revealed many cases of strong neutron-proton symmetry breaking for  $E2$  excitations, and several sharp departures from

symmetry also for  $E3$  examples [9]. The unusual and unexpected behavior of electric quadrupole ( $E2$ ) collective excitations in some strongly collective nuclei led us to question what would be observed if the relatively weak  $E2$  excitations near closed shells were observed. That is, how rapidly do these asymmetries in neutron and proton roles in collective excitations develop?

Recent shell model calculations for both  $^{204,206}\text{Pb}$  attributed all known levels up to about 3 MeV excitation [10] as valence neutron-hole excitations, and those calculations were quite successful in describing energies and electromagnetic (EM) transition rates using effective charges, except for  $3^-$  levels. Thus an experiment to explore the weakly collective excitations in  $^{204}\text{Pb}$  and  $^{206}\text{Pb}$ , and to examine hadron dependence of excitation strengths, was undertaken.

It should also be useful to compare these collective excitation strengths to those for  $^{208}\text{Pb}$ , where there are no evident valence excitations. Since valence neutrons dominate the low-lying structure of the two lighter Pb isotopes [10,11], neutron scattering should see enhanced quadrupole coupling strengths when compared to Coulomb excitation; but that might not be the case for  $^{208}\text{Pb}$  [8,12].

It seemed desirable to ascertain not only the  $E2$  strengths in the two above-mentioned Pb isotopes, but also their  $3^-$  strengths. Earlier Cottle *et al.* [13] had argued that the  $3^-$  strength held quite well collected into a single excited level in the even-even nuclei below  $^{208}\text{Pb}$  until one reached  $^{196}\text{Pt}$ ; the strength in the lowest  $3^-$

\*Present address: Booz, Allen and Hamilton, 1525 Perimeter Parkway, Huntsville, AL 35806.

<sup>†</sup>IBM, 1 Kirkwood Blvd., Roanoke, TX 76299.

<sup>‡</sup>Nuclear Physics Division, China Institute of Atomic Energy, Beijing, P. O. Box 275(46), 10234 Beijing, People's Republic of China.

level there is much weaker than that in even  $A$  nuclei closer to  $^{208}\text{Pb}$ . We wished to measure the  $3^-$  strength in the two Pb isotopes, as excited in neutron scattering, and compare it to the strength found by other excitation methods [14]. The  $3^-$  excitations were those least well characterized as valence neutron excitations in the shell model calculations [10].

Recent studies of these Pb excitations have been made in intermediate energy  $^{17}\text{O}$  scattering [15] and in pion scattering [16]. The  $^{17}\text{O}$  studies show that the strong low energy fragment of the giant quadrupole resonance near 4 MeV excitation is nearly pure isoscalar in all three Pb isotopes mentioned above, while the first excited  $2^+$  levels in the two lighter isotopes are indeed dominated by target neutron excitations, or have strong isovector components. They find also that the  $3^-$  excitations, the strongest of all collective excitations in these nuclei, are approximately pure isoscalar excitations; they do not seem to reflect at all the dominance of valence neutron excitations observed for  $E2$  excitations.

These conclusions are reached by detailed examination of Coulomb-nuclear interference patterns in inelastic oxygen ion scattering. Further, one must assume that the interaction strength of the incoming heavy ion with target neutrons is of the same strength as that with the target protons, in order to interpret the nuclear scattering amplitude [15], and that the oxygen mean scattering field has been well determined by fitting the elastic and inelastic scattering cross sections. The first assumption seems self-evident in the case of  $i$  spin-zero projectiles, such as  $\alpha$  particles or  $^{16}\text{O}$  ions, but may not be quite so evident for  $^{17}\text{O}$  ions, with a valence neutron well outside the  $^{16}\text{O}$  core.

It seems profitable to test hadron dependence in scattering studies of collective excitations using nucleons, since the interaction strengths of incoming neutrons and protons with nuclei has been exhaustively studied and fixed [8,12] over a quite wide energy range for both nucleons, and mean scattering fields are often very well determined for nucleon scattering. Inelastic scattering cross sections depend on the direct coupling strengths which we seek; but the cross sections depend sensitively not only on them, but also upon the mean scattering fields which perturb projectile and ejectile amplitudes near the nuclear surface. Thus, to extract these coupling strengths reliably, it is necessary to fix the mean scattering fields well. To this end it has been common practice in this and other laboratories to use many scattering observables to constrain neutron mean fields [1,3,17], including total cross sections over an extended range of incident energies and differential scattering cross sections at several incident energies. This procedure was followed in this study.

There is an additional reason for interest in mean scattering fields for these nuclei. It has been noted in several experiments [18,19] that dispersion-corrected scattering fields allow observers to connect scattering potentials to those needed to represent bound single-particle strengths. Following the procedures developed by Mahaux and Ngo [20] and others [18,21] the dispersion corrections have indeed allowed consistent potential developments between fairly high energy scattering and bound single particle strengths. But many of the spherical model (SOM) potential descriptions have suffered from not being able to include quite low energy scattering in the same consistent description [18,19]. On the other hand, coupled channels models (CC) have for several nuclei enabled bound states, low-energy scattering and higher-energy observables to be successfully represented in a single mean field representation [19,22]. We thought comparing the success of SOM and CC approaches to developing dispersion-corrected mean fields for the two Pb isotopes would be useful.

A large set of scattering data is needed to accomplish the objectives noted above. Differential scattering cross sections were thus measured at incident neutron energies of 2.5, 4.6, and 8.0 MeV for both  $^{204,206}\text{Pb}$ . Elastic and inelastic scattering cross sections to the first few excited states were measured at 15–20 angles at each incident energy. Further, neutron total cross sections for both  $^{204,206}\text{Pb}$  were measured between 250 keV and 4 MeV in steps of about 100 keV with an energy resolution of about 50 keV for both isotopes.

## II. EXPERIMENTAL METHODS

Two different sets of measurements were performed at the University of Kentucky, requiring two different experimental arrangements and methods. One arrangement was used to provide total cross sections over the incident neutron energy range from 250 keV to 4 MeV. [23,24] The other system was used for measurements of differential scattering cross sections at 2.5, 4.6, and 8.0 MeV. All measurements with either arrangement employed the same separated isotope scattering samples. The samples were metallic cylinders with dimensions, isotopic enrichments, and masses given in Table I.

### A. Total cross sections

The purpose of measuring total cross sections is to provide essential information for development of an energy-dependent mean scattering field, as noted above. Total

TABLE I. Sample dimensions and isotope abundances

Sample	Physical characteristics		Percent isotope abundance			
	Mass	Dimensions	$^{204}\text{Pb}$	$^{206}\text{Pb}$	$^{207}\text{Pb}$	$^{208}\text{Pb}$
$^{204}\text{Pb}$	45.9 g	$h=2.1$ cm, $d=1.6$ cm	71.4	12.5	6.3	9.8
$^{206}\text{Pb}$	58.3 g	$h=2.0$ cm, $d=1.8$ cm	0.0	88.6	8.5	2.9

cross sections below 250 keV neutron energy would not have been especially helpful, as the total cross sections below that energy exhibit strong isolated resonance effects.

The total cross section arrangement and methods used at the University of Kentucky are discussed in detail in Ref. [23] and [24]; only a brief description will be given here. The  $^3\text{H}(p,n)^3\text{He}$  neutron source was shielded with a forced reflection collimation system, which formed a neutron flux with diameter 0.8 cm at  $0^\circ$  from the incident proton beam. Samples were positioned just beyond the 1 m long forced reflection incident flux collimator, and the detector was 2 m beyond the sample, with a collimated aperture of 1.5 cm diameter. This geometry was good enough that corrections for multiple, or in-scattering were well below 1%, and thus negligible. Corrections were made for the effects of resonance or sample self-shielding [25,26]; these corrections were  $\leq 10\%$  at 1 MeV and negligible above 2 MeV. The total experimental uncertainty was found to be less than 2%, which was verified by measuring the neutron total cross sections of carbon at several neutron energies. The carbon cross section is known to better than 1% in this energy region [27]. The energy resolution was 100 keV below 0.5 MeV, and less than 50 keV at 4 MeV.

Our measurements for  $^{206}\text{Pb}$  overlapped those of Horen *et al.* [28] near 4 MeV and agreed with the ORELA results to within better than 1%. The ORELA measurements covered the energy range from 4 MeV to about 8 MeV. Thus combining the present and ORELA results gave us a total cross section set for  $^{206}\text{Pb}$  from 400 keV to 8 MeV with an accuracy of about 2%.

## B. Differential cross section methods

The experimental methods used at the University of Kentucky for measurements of differential scattering cross sections have been well described in several recent publications [1,17,29]. Hence, only details pertinent to the  $^{204,206}\text{Pb}$  measurements are given here. The  $^3\text{H}(p,n)^3\text{He}$  reaction was again used as a source of neutrons for incident energies below 5 MeV, while the  $^2\text{H}(d,n)^3\text{He}$  reaction was used at 8 MeV. The scattering samples were hung 7.5, 8.0, and 7.5 cm from the center of a hydrogen-containing gas cell for the 2.5-, 4.6-, and 8.0-MeV scattering experiments, respectively. A shielded neutron scintillation detector was mounted a fixed distance from the scattering sample such that neutrons scattered from the low-lying levels of  $^{204,206}\text{Pb}$  could be separated using time-of-flight (TOF) techniques. The flight paths for the three experiments were 3.00, 3.95, and 3.88 m, while the energy resolution was 72, 108, and 228 keV at 2.5-, 4.6-, and 8.0-MeV incident neutron energies, respectively. Typical scattering spectra measured at 2.53 MeV incident are shown in Fig. 1.

Yields were extracted from the TOF spectra with a fitting program that positions scattering peaks to maintain energy separations fixed by kinematics. Each peak is fitted with an asymmetric form which properly accounts for both fixed energy and time spreads in the experiments.

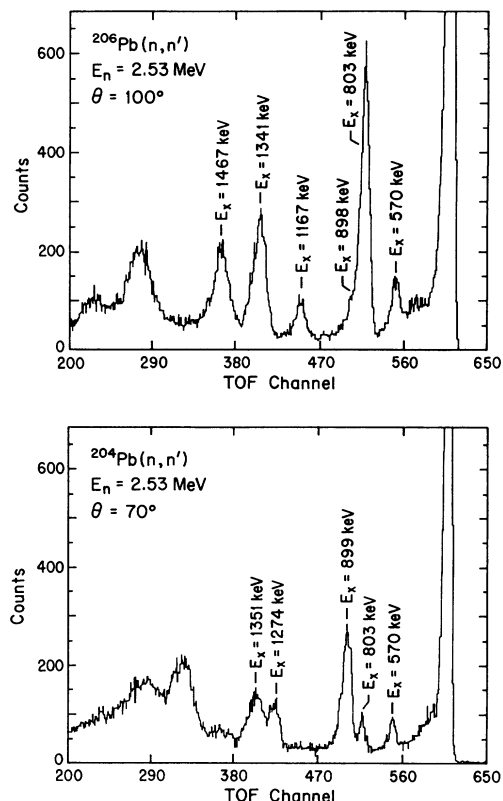


FIG. 1. Scattered neutron spectra at  $70^\circ$  and 2.53 MeV incident. The top panel provides the spectrum for  $^{206}\text{Pb}$ , with excitation energies of levels indicated, while the lower panel presents the same for  $^{204}\text{Pb}$ . At this energy most levels are comparably excited, having large CS cross sections.

The data were then corrected for electronic deadtime and for effects due to the finite size of the scattering sample. The sample-size corrections were made using an updated form [30] of the forced collision Monte Carlo computer code [31] MULCAT. Included were the usual corrections for neutron attenuation and multiple scattering.

The corrected scattering yields for incident energies of 2.5 and 4.6 MeV were normalized to cross sections through yields measured also for a C scattering sample, and normalized to the evaluated cross-section file [27]. At these energies the angle-integrated scattering cross sections are also the total cross sections [32], and are known to better than  $\pm 1\%$ . The measured yields at 8 MeV incident were normalized both to the n,p scattering cross sections from the Breit-Hopkins evaluation [33], which are known to much better than  $\pm 1\%$ , and to C scattering cross sections. Yields for (n,p) scattering were measured with a 1 cm x 0.32 cm diameter polyethylene sample. Hydrogen scattering yields were measured at  $30^\circ$ ,  $40^\circ$ , and  $50^\circ$ . Although the elastic scattering cross sections for C have uncertainties [34] of  $\pm 4.5\%$ , the carbon and hydrogen normalizations agreed with each other to within about 2%.

## C. Isotopic corrections

Incomplete isotopic enrichments, or isotopic contaminants, were a special problem in this experiment, since

the isotopic enrichments of our scattering samples were not especially high. These Pb samples, particularly the 71.4% enriched  $^{204}\text{Pb}$  sample, had sizable contributions from other than the most abundant isotope. Fortunately good total cross sections files exist to serve as the basis of corrections [35–38]. Tables of these authors' cross sections are on file at the National Nuclear Data Center (NNDC). These files were used with our normalized and corrected yields first to unfold the  $^{207}\text{Pb}$  and  $^{208}\text{Pb}$  cross sections from the  $^{206}\text{Pb}$  sample yields and thus determine  $^{206}\text{Pb}$  cross sections; then those cross sections together with the NNDC data files enabled separation of the  $^{204}\text{Pb}$  cross sections from the yields for that sample.

The problem of unfolding the separated isotope elastic and inelastic differential scattering cross sections was particularly important at 2.5 MeV incident energy, where the compound system (CS) cross section components were large and different for each isotope. Fortunately differential scattering cross sections exist for scattering from  $^{207}\text{Pb}$  and  $^{208}\text{Pb}$ . These have been reported by Refs. [39] and [40] respectively. The differential cross sections files are also available from NNDC. Most of the inelastic scattering groups for scattering to levels of the different isotopes were separated in the TOF spectra; thus the correction for those was simply dividing the yields by the appropriate isotopic abundance. The 899-keV level of  $^{204}\text{Pb}$  was not separated from the 898-keV yield of  $^{207}\text{Pb}$ . At 2.5 MeV cross sections [39] from the NNDC files were used for the 898-keV  $^{207}\text{Pb}$  level and at 4.6 MeV we were able to extract  $^{207}\text{Pb}$  inelastic yields from our  $^{206}\text{Pb}$  data, and use these to correct yields for the 899-keV level of  $^{204}\text{Pb}$ .

Uncertainties contributed by this unfolding process are no larger than 1–2% except in the minima at 2.5 MeV where CS effects are most important; there uncertainties are estimated to be < 5%. Corrections are quite small since the cross sections for the different isotopes are similar, especially when CS contributions become negligible. These abundance corrections could not be made at 8 MeV except for elastic scattering, because  $^{207}\text{Pb}$  inelastic data do not exist near that energy. In cases where the levels could not be resolved and there were no existing data, the masses of all contributing isotopes were used in determining the cross sections. For example, at 8 MeV the entire sample mass was used in calculating the  $3^-$  cross sections. The uncertainty in this procedure is estimated to be quite low since the octupole excitation strengths are found to be approximately equal for the Pb isotopes.

### III. ANALYSES WITH SOM AND CC MODELS

#### A. Spherical model analyses

We begin the analyses of  $^{204,206}\text{Pb}$  with a SOM analysis since these nuclei are semimagic. The assumption of a spherical shape should be appropriate, especially for determining potential parameters and CS or statistical model cross sections. Additionally, the scattering field derived from the SOM analyses should be similar to that

needed for the strong coupling approach to describing low-energy scattering from these nuclei [41]. This CC model will be addressed in the next section.

The computer code OPSTAT [42], which can calculate both shape elastic or direct and compound elastic cross sections simultaneously, was used for this analysis. CS cross sections are especially important for the low-energy data at 2.5- and 4.6-MeV incident energy where few levels are excited, but are negligible at 8.0 MeV.

Width-fluctuation and resonance-resonance correlation corrections to the statistical model or CS cross sections, as proposed by Hofmann *et al.* [43], were used in all CS calculations. Calculated CS cross sections can be checked against measured inelastic scattering cross sections at both 2.5- and 4.6-MeV incident energy. Several of the scattering cross sections, including scattering to the  $4_1^+$  and  $2_2^+$  levels in  $^{204}\text{Pb}$  and the  $3_1^+$  and  $2_2^+$  levels in  $^{206}\text{Pb}$ , have negligible direct excitation components and can be used to test our CS calculations. These CS calculations have no free parameters once the scattering potential has been parameterized to fit total and differential elastic scattering cross sections. Thus comparisons between calculated and measured cross sections provide an excellent test of the model. Agreement between these measured cross sections and the corresponding CS calculations was always well within the established uncertainties of the measured cross sections. Some of these data and the corresponding CS calculations are shown in Figs. 2 and 3 for scattering from the levels mentioned above

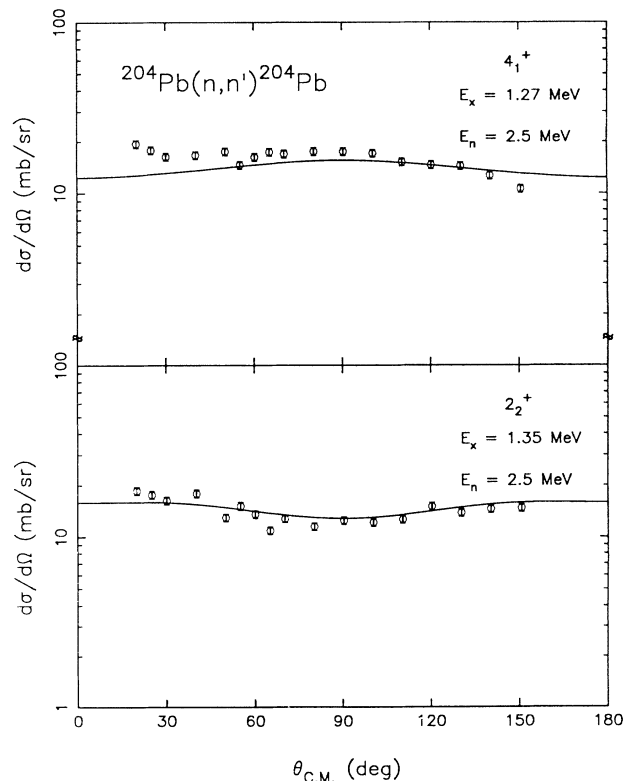


FIG. 2. Neutron inelastic scattering cross sections from the  $4_1^+$  and  $2_2^+$  levels of  $^{204}\text{Pb}$  measured at an incident energy of 2.5 MeV are presented in the upper and lower panels, respectively. The solid curves represent the calculated compound nuclear cross sections.

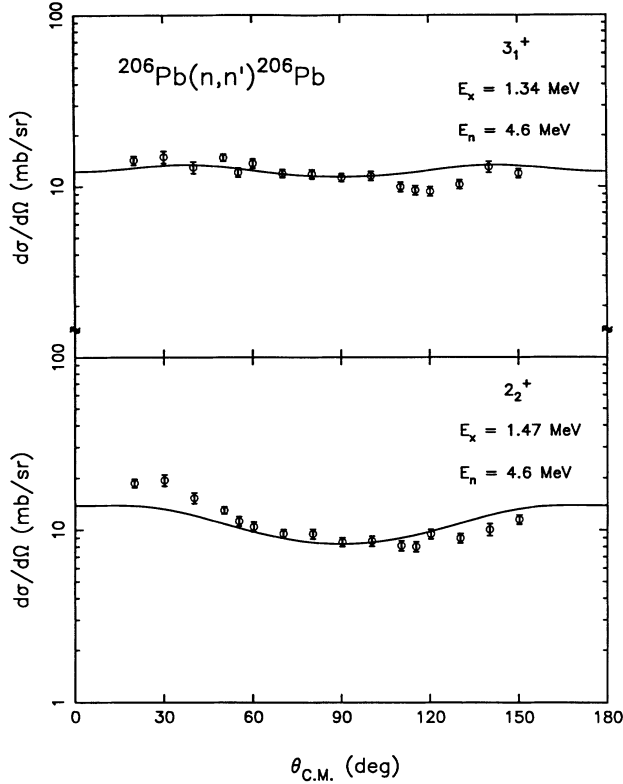


FIG. 3. Inelastic scattering cross sections from the  $3_1^+$  and  $2_2^+$  levels of  $^{206}\text{Pb}$  measured at an incident neutron energy of 4.6 MeV are presented in the upper and lower panels, respectively. The solid curves represent the calculated compound nuclear cross sections.

$^{204,206}\text{Pb}$ .

The form of the optical model potential used in these analyses was the usual Woods-Saxon shape for the real potential, and derivative Wood-Saxon for surface imaginary and spin-orbit terms. Searching on potential pa-

rameters for both Pb isotopes to develop the best overall fit to the total cross sections from 250 keV to 8 MeV, and for the differential elastic scattering cross sections for neutron energies of 2.5, 4.6, and 8 MeV, brought the result that little energy dependence of geometry parameters was indicated to achieve the best results. The best real diffuseness for 8 MeV was about 10% less than that which worked best for total cross sections at 2 MeV and differential elastic scattering cross sections at 2.5 MeV. However, this difference is small, and the energy region fitted was not extensive enough to call for energy dependent geometries. Thus all analyses used fixed geometries.

The potential parameters deduced from these spherical analyses are given in Tables II and III for  $^{204}\text{Pb}$  and  $^{206}\text{Pb}$ , respectively. The solid curves fitting the total cross sections in Fig. 4 were prepared with these parameters. Total cross sections for both isotopes are strongly affected by resonance structure below approximately 1 MeV. The SOM curves of Fig. 4 are in excellent agreement with the data above 1 MeV, where residual fluctuations are negligible.

The strength of the real scattering potentials is found to be approximately constant with energy below 2.5 MeV, and rises to a maximum at energies less than about 5 MeV. It decreases with a rate often found for scattering potentials above 4.6 MeV [44]. The energy dependence of the real scattering potential is just that which would reflect a combination of a Hartree-Fock potential and dispersion corrections [19] arising from the energy dependence of the imaginary or absorptive potentials.

Comparisons of the SOM calculations with the neutron elastic scattering differential cross sections are shown as solid lines in Figs. 5 and 6 for  $^{204}\text{Pb}$  and  $^{206}\text{Pb}$ , respectively. The calculations are in good agreement with the data for both isotopes at all three incident neutron energies, 2.5, 4.6, and 8.0 MeV. The potentials given in Tables II and III are constrained to fit simultaneously both the neutron differential elastic scattering cross sec-

TABLE II.  $^{204}\text{Pb}$  neutron scattering potentials for both SOM and first-order vibrational models (FOV). The  $^{204}\text{Pb}$  neutron scattering potential developed in conjunction with models as described in the text. The symbol  $V$  denotes the real potential depth;  $W_D$  denotes surface absorptive depth;  $V_{\text{so}}$  means real spin-orbit depth. All potential depths are specified in MeV. The radius parameters ( $r$ ) and diffusenesses ( $a$ ) are given in fermis,  $r$  as a coefficient of  $A^{1/3}$ . Below 2.5 MeV, the real potential is energy independent. The geometry is common to both models.

		SOM potential parameters		
$V =$	44.58	$E < 2.5$ MeV	$r_r = 1.28$	$a_r = 0.65$
	$44.09 + 0.19E$	$2.5 < E < 4.6$ MeV		
	$47.84 - 0.62E$	$E \geq 4.6$ MeV		
$W_D =$	$4.28 + 0.71E$	$E \leq 4.91$	$r_{W_D} = 1.28$	$a_{W_D} = 0.41$
	$8.41 - 0.13E$	$E > 4.91$		
$V_{\text{so}} =$	7.10		$r_{\text{so}} = 1.01$	$a_{\text{so}} = 0.45$
		FOV model potential parameters		
$V =$	44.50	$E \leq 2.5$ MeV	$r_r = 1.28$	$a_r = 0.65$
	$43.74 + 0.30E$	$2.5 < E < 4.6$ MeV		
	$47.47 - 0.51E$	$E \geq 4.6$ MeV		
$W_D =$	$3.53 + 0.59E$	$E \leq 2.53$ MeV	$r_{W_D} = 1.28$	$a_{W_D} = 0.41$
	$7.40 - 0.11E$	$E > 2.53$ MeV		
$V_{\text{so}} =$	7.10		$r_{\text{so}} = 1.01$	$a_{\text{so}} = 0.45$
Coupling parameters		$\beta_2^{n,n'} = -0.044$	$\beta_3^{n,n'} = 0.12$	
		$\beta_2^{\text{em}} = 0.038$	$\beta_3^{\text{em}} = 0.11$	

TABLE III.  $^{206}\text{Pb}$  Neutron Scattering Potentials for both SOM and first-order vibrational models (FOV). The  $^{206}\text{Pb}$  neutron scattering potential developed in conjunction with models as described in the text. The symbol  $V$  denotes the real potential depth;  $W_D$  denotes surface absorptive depth;  $V_{\text{so}}$  means real spin-orbit depth. All potential depths are specified in MeV. The radius parameters ( $r$ ) and diffusenesses ( $a$ ) are given in fermis,  $r$  as a coefficient of  $A^{1/3}$ . Below 2.5 MeV, the real potential is energy independent.

		SOM potential parameters		
$V =$	44.95	$E < 2.5$ MeV	$r_r = 1.27$	$a_r = 0.62$
	$44.56 + 0.15E$	$2.5 < E < 4.6$ MeV		
	$47.84 - 0.56E$	$E \geq 4.6$ MeV		
$W_D =$	$3.32 + 0.55E$	$E < 6.42$	$r_D = 1.28$	$a_{W_D} = 0.41$
	$7.62 - 0.12E$	$E \geq 6.42$		
$V_{\text{so}} =$	7.10		$r_{\text{so}} = 1.01$	$a_{\text{so}} = 0.45$
		FOV model potential parameters		
Potential depths				
$V =$	45.15	$E \leq 2.5$ MeV	$r_r = 1.27$	$a_r = 0.60$
	$44.40 + 0.30E$	$2.5 < E < 4.6$ MeV		
	$48.15 - 0.52E$	$E \geq 4.6$ MeV		
$W_D =$	$2.87 + 0.48E$	$E \leq 5.52$ MeV	$r_D = 1.28$	$a_{W_D} = 0.41$
	$6.01 - 0.09E$	$E > 5.52$ MeV		
$V_{\text{so}} =$	7.10		$r_{\text{so}} = 1.01$	$a_{\text{so}} = 0.45$
Coupling parameters		$\beta_2^{n,n'} = -0.040$	$\beta_3^{n,n'} = 0.12$	
		$\beta_2^{\text{cm}} = 0.030$	$\beta_3^{\text{cm}} = 0.11$	

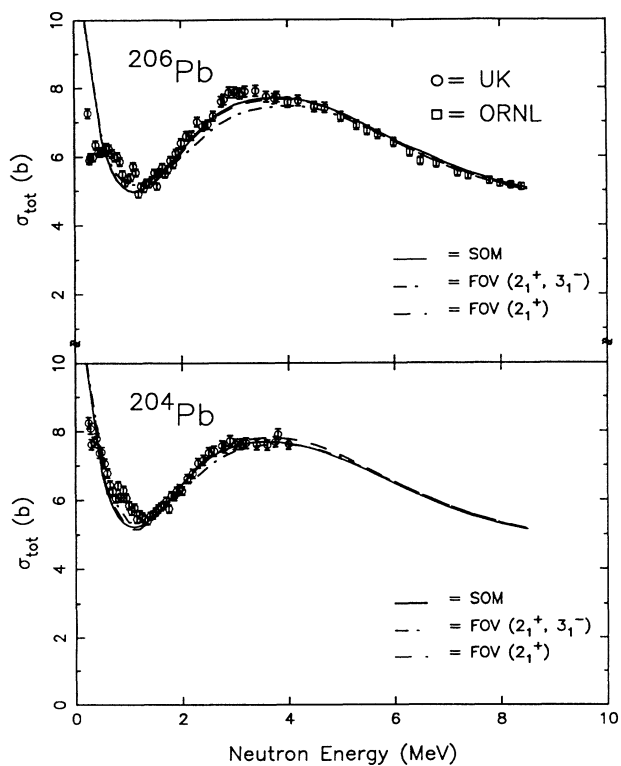


FIG. 4. Neutron total cross sections measured between 250 keV and 8.0 MeV are presented for  $^{206}\text{Pb}$  in the top panel of the figure, and from 250 keV to 4 MeV for  $^{204}\text{Pb}$  in the bottom panel. The curves represent optical model calculations as discussed in the text.

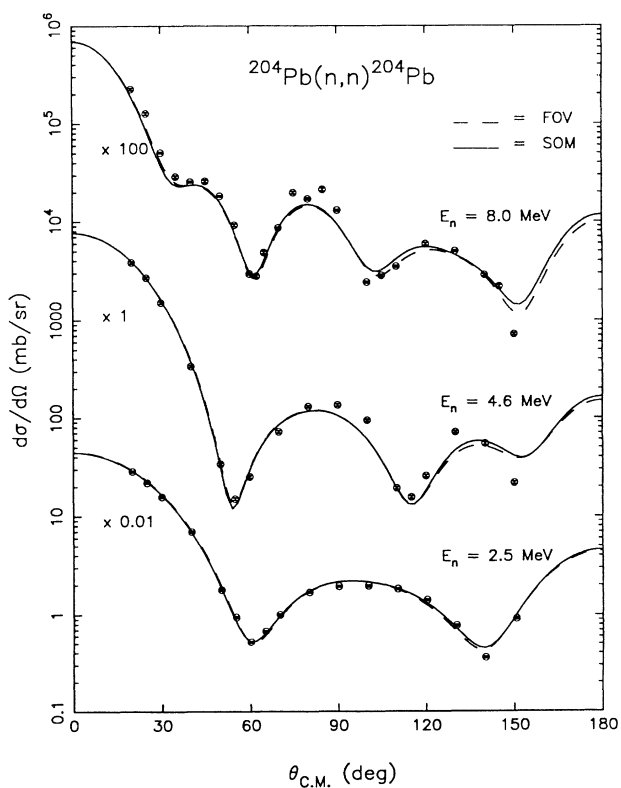


FIG. 5. Neutron elastic scattering cross sections from  $^{204}\text{Pb}(n,n)^{204}\text{Pb}$  are presented at incident energies of 2.5, 4.6, and 8.0 MeV. The curves are from optical model calculations as discussed in the text.

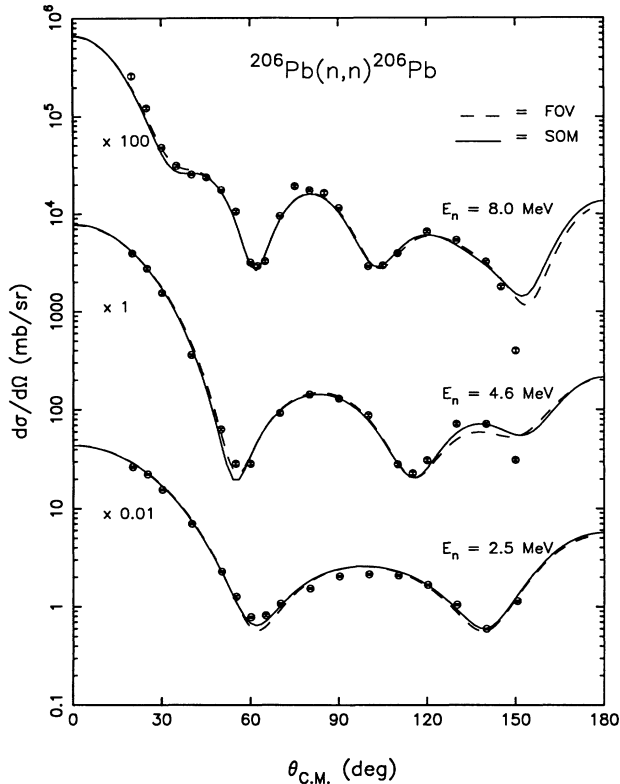


FIG. 6. Neutron elastic scattering cross sections from  $^{206}\text{Pb}$  are presented at incident energies of 2.5, 4.6, and 8.0 MeV. The curves are from optical model calculations as discussed in the text.

tions as well as the total cross sections. CS components to the elastic scattering cross sections are included in all calculations but are not shown explicitly.

We find that a SOM adequately describes the measured neutron elastic scattering and neutron total cross sections between 250 keV and 8 MeV, as well as many inelastic scattering cross sections, as is shown in the several figures indicated. These good results obtained with single channel (SOM) models for Pb isotopes contrast with results from scattering for strongly collective nuclei [1,2]. The spherical or single channel models failed badly to describe elastic scattering and total cross sections for those nuclei. The proximity of these Pb nuclei to rigid, spherical  $^{208}\text{Pb}$ , and the general weakness of direct coupling to inelastic channels in these Pb nuclei has the result that SOM models will work rather well. Not well described by a spherical model and CS cross sections are the  $2_1^+$  and  $3_1^-$  cross sections, which have large direct excitation components. Dealing with those cross sections in the context of all scattering is the focus of the next section.

### B. Coupled channels analyses

A first-order vibrational model (FOV) was used to couple the  $2_1^+$  and  $3_1^-$  excited levels mentioned above to

the elastic scattering channels in our CC analyses. The quadrupole and octupole coupling strengths,  $\beta_2^{nn'}$  and  $\beta_3^{nn'}$ , for the  $2_1^+$  and  $3_1^-$ , respectively, were determined by obtaining good fits to the inelastic scattering cross sections to these two levels while maintaining the successes of the SOM in describing other scattering data. The well-known code [45] ECIS79 was used for these CC calculations. Neglecting all excited levels but these in our CC model seems well justified, since other high-lying states exhibit little direct excitation at our incident energies.

Neutron scattering potentials for  $^{204,206}\text{Pb}$  of the SOM served as the starting point in our CC analyses, since major differences are not expected in going from SOM to FOV models [41]. The largest change is expected to be in the strength of the absorptive potential, since two major inelastic excitations are treated explicitly, rather than being included in the effects of the absorptive potential. Fortunately the code ECIS79 enables calculation of direct coupling and CS cross sections consistently, within a single representation. This is particularly important to analyses and interpretation at the two lower incident energies of this experiment, where CS cross sections are rather large. In practice the CS cross sections of the CC model were not very different than those of the SOM model, for as is evident in Tables II and III even the imaginary absorptive potentials are not very different for the two models.

Initial quadrupole and octupole coupling strengths,  $\beta_2^{\text{em}}$  and  $\beta_3^{\text{em}}$ , were taken from EM studies [14,46]. The strengths of the real and imaginary potentials were searched to provide good fits to the elastic scattering cross sections at all three incident neutron energies, as shown by the dashed lines in Figs. 5 and 6. These fits to the elastic scattering cross sections were maintained throughout the CC analyses by varying the depth of the absorptive potentials as the coupling strengths were adjusted. Corresponding fits to the total cross sections are given by the dashed and dot-dashed lines shown in Fig. 4.

Calculations for scattering to the  $2_1^+$  levels at 8-MeV incident energy using  $\beta_2^{\text{em}}$  are shown in Figs. 7 and 8 as the dashed curves for  $^{204}\text{Pb}$  and  $^{206}\text{Pb}$ , respectively. These calculations are badly below the data, and  $\beta_2^{nn'}$  had to be increased by 33% and 15% over  $\beta_2^{\text{em}}$  for  $^{206}\text{Pb}$  and  $^{204}\text{Pb}$ , respectively, to provide good agreement with the neutron scattering cross sections. The results of those changes of coupling strength are shown as the solid curves in Figs. 7 and 8; the absorptive potential was correspondingly reduced from that of the SOM model so that good fits to the elastic scattering and total cross sections were always maintained. Similar calculations are shown for 4.6 MeV and 2.5 MeV in Figs. 7 and 8. Exactly the same quadrupole coupling strengths were needed to fit the 4.6 and 8.0 MeV data for both  $^{204,206}\text{Pb}$ , but attempts to represent the 2.5 MeV inelastic scattering data to the  $2_1^+$  levels led to higher values for  $\beta_2$  at that energy. This is the only incident energy where CS components were quite large, even larger than the direct coupling components. Uncertainty in corrections for isotopic abundances were important, because the CS cross sections for

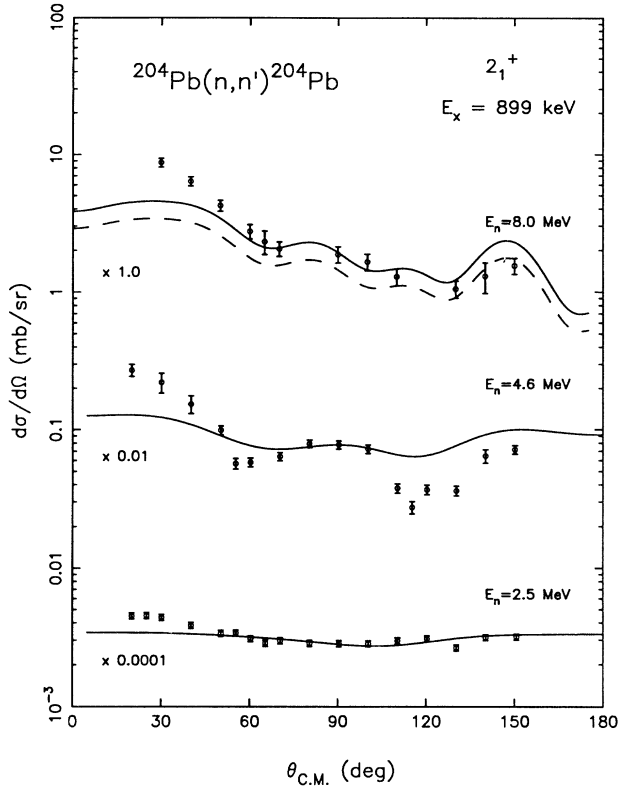


FIG. 7. Neutron inelastic scattering cross sections from the  $2_1^+$  level of  $^{204}\text{Pb}$  measured at incident energies of 2.5, 4.6, and 8.0 MeV. The solid curves are from CC calculations which use  $\beta_2 = -0.044$ . The dashed curve, shown only at 8 MeV, uses the coupling strength determined from em excitation studies; i.e.,  $\beta_2^{\text{em}} = 0.038$ .

$^{207}\text{Pb}$  were substantially less than those for the even- $A$  isotopes, owing to the larger number of levels excited in the odd- $A$  nuclide. Thus the apparently higher  $\beta$  values at this energy probably reflects inadequate information for isotopic abundance corrections, which would pose a particular problem for separating direct coupling and CS components at this low energy, where the CS cross sections are large.

Octupole strengths were extracted from scattering cross sections for the  $3_1^-$  levels of  $^{204,206}\text{Pb}$  at an incident energy of 8 MeV. Values consistent with this were found at 4.6 MeV, but CS contributions from unresolved levels prohibited an unambiguous determination of  $\beta_3^{n'}$  at this energy. The results of these CC calculations for the  $3_1^-$  levels are shown as solid curves in Fig. 9. The extracted direct coupling or scattering amplitudes for octupole excitations are represented by the  $\beta_3$  values, which were found to be about 12% to 13% larger than those extracted from EM excitation [14].

The final potential parameterizations for the CC model are presented in Tables II and III along with those of the SOM. One can note there that the SOM and CC potential parameter sets are very similar to each other, as expected for relatively weak, first order coupling. The  $\beta$  values for both quadrupole and octupole excitations are presented with their EM counterparts and with potential

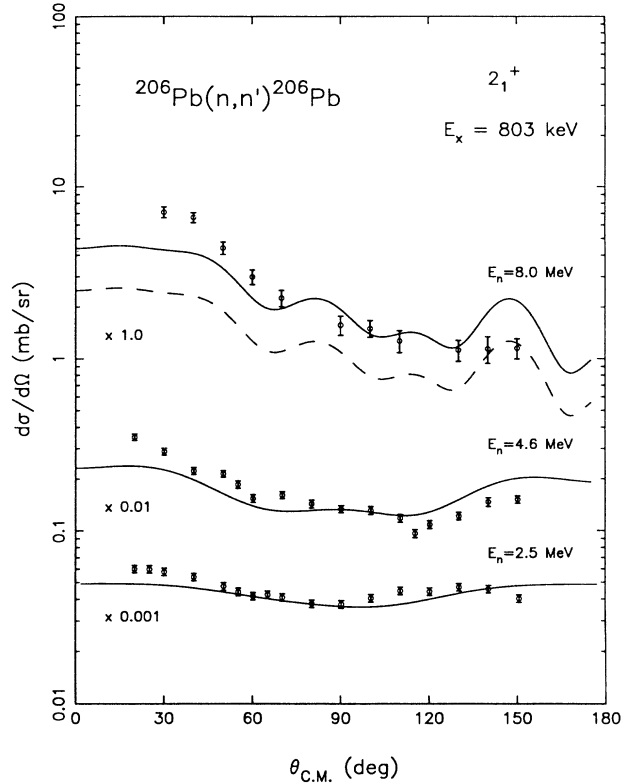


FIG. 8. Neutron inelastic scattering cross sections from the  $2_1^+$  level of  $^{206}\text{Pb}$  measured at incident energies of 2.5, 4.6, and 8.0 MeV. The solid curves are from CC calculations which use  $\beta_2 = -0.04$ . The dashed curve, shown only at 8 MeV, uses the coupling strength determined from em excitation studies; i.e.,  $\beta_2^{\text{em}} = 0.03$ .

parameters in Tables II and III. Uncertainties of these extractions are judged to be about  $\pm 2\%$ . The  $\beta$  parameters listed there are referred to the radii of our neutron scattering analyses. The sign of the coupling strengths cannot be determined within the FOV model, although a negative sign for  $\beta_2$  is consistent with other measurements in this mass region [23].

The  $\beta_3^{n'}$  values extracted are consistent with a single value for both isotopes, and one about 13% stronger than that determined in electron scattering or Coulomb excitation experiments [14]. This difference is significant since it indicates that neutron scattering sees a different amplitude than does EM excitation. Scattering cross sections of Annand *et al.* [19] for the  $3^-$  level of  $^{208}\text{Pb}$  were re-analyzed by Cheema and Finlay [47] using DWBA methods to obtain the  $E3$  coupling strength independent of the incident energy. We note that the value we have found for  $^{204,206}\text{Pb}$  is about 6% larger than the value extracted for scattering from  $^{208}\text{Pb}$ . The same difference between a common EM value for  $^{204,206}\text{Pb}$  and an about 6% smaller EM value for  $^{208}\text{Pb}$  also obtains [14].

#### IV. INFERENCES FOR TARGET PROTONS AND NEUTRONS

The quantitative enhancements of neutron scattering amplitudes over EM amplitudes for both quadrupole and



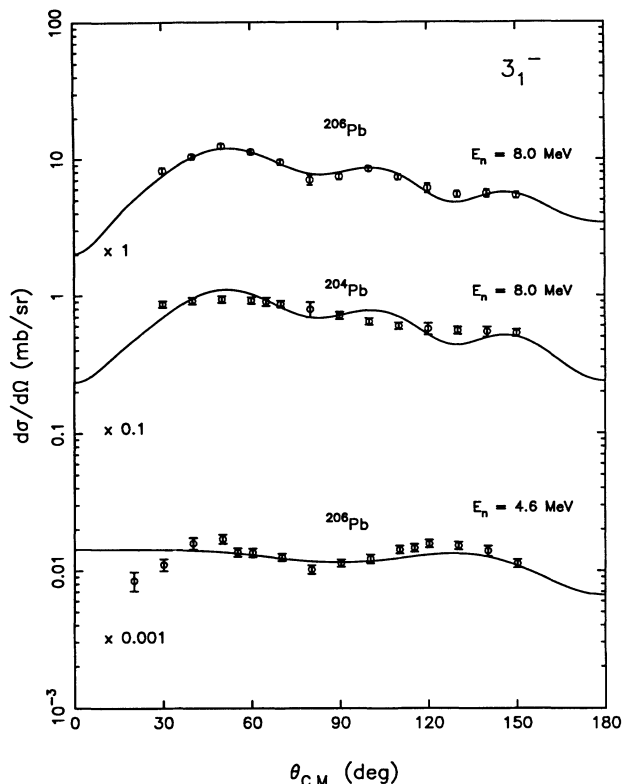


FIG. 9. Neutron inelastic scattering cross sections from the  $3_1^-$  level of  $^{206}\text{Pb}$  measured at incident energies of 4.6 and 8.0 MeV and from the  $3_1^-$  of  $^{204}\text{Pb}$  at 8.0 MeV. The solid curves are from CC calculations which use  $\beta_3 = 0.121$  for  $^{204}\text{Pb}$  and  $\beta_3 = 0.120$  for  $^{206}\text{Pb}$ .

octupole excitations for the two isotopes can be nicely interpreted in terms of nuclear structure matrix elements for exciting target neutrons,  $M_n$ , and target protons,  $M_p$ . The model for this separation has been independently developed by Brown, Bernstein, and Madsen and their colleagues from 1975 to 1981 [8], and in an essentially equivalent model provided by Alons *et al.* [12]. Paraphrasing the results of the two groups, and using a notation drawn from both references, we write:

$$\frac{\delta_\ell^{nn'}}{\delta_\ell^{em}} = \left[ \frac{(\chi_{np}M_p + \chi_{nn}M_n)/(\chi_{np}N_p + \chi_{nn}N_n)}{M_p/N_p} \right]_\ell,$$

where  $\chi_{np}$  is a weight factor for the effective neutron-proton interaction strength,  $\chi_{nn}$  is a similar factor for the neutron-neutron interaction strength,  $\delta_\ell^{nn'}$  is the collective model deformation length deduced from our neutron scattering data, and  $\delta_\ell^{em}$  is deduced from measured EM transition probabilities. The parameter  $\ell$  denotes the multipolarity of the transition. These deformation parameters are related to experimental coupling strengths by  $\delta = \beta R$ . This ratio may be rewritten so that it only involves the ratio of the interaction strengths, and the ratio  $M_n/M_p$ . The other weights are  $N_p$  and  $N_n$ , the numbers of protons and neutrons, respectively, presumed to be participating in the excitations. Only the ratio of these weights is involved in the comparison of EM and neutron scattering amplitudes. But it is conventional,

absent specific models to the contrary, to present even low-lying collective excitations as belonging to the entire nucleus. Thus this ratio,  $N_n/N_p$ , is usually replaced by  $N/Z$ , the total number of neutrons divided by the total number of protons in the nucleus. This is quite appropriate for giant resonances, as advanced recently for these Pb nuclei by Horen *et al.* [15,16] but may be less realistic for the two low-lying excitations studied here.

We may rewrite the ratio above:

$$\frac{\delta_\ell^{nn'}}{\delta_\ell^{em}} = \left[ \frac{(\chi_{np}/\chi_{nn} + M_n/M_p)}{\chi_{np}/\chi_{nn} + N/Z} \right]_\ell.$$

The normalization concept of this ratio is that if all particles participate equally in an excitation, then the ratio will be 1, and the matrix element per valence particle would be the same for neutrons as for protons. This is what is found always for well-deformed rotors. Using this formula, the calculated ratio  $M_n/M_p$  is extracted for the  $2_1^+$  and  $3_1^-$  levels of the two isotopes, for comparison with similar ratios calculated from interference amplitudes in  $^{17}\text{O}$  scattering [15], and for  $^{206}\text{Pb}$  also in comparisons of  $\pi^+$  to  $\pi^-$  scattering [16]. Generally there is good agreement among the three experiments, as shown by the ratios of  $M_n/M_p$  tabulated in Table IV.

Since an extensive effort has been made to determine accurately the mean scattering field in this experiment, the uncertainty of the ratios from this work is judged to be about  $\pm 6\%$ . For reference, we compare all ratios to  $N/Z$ , which for these two Pb nuclei is  $N/Z \simeq 1.5$ . Were one to argue that only the last (closed) shell of neutrons and protons appreciably participated, in addition to the neutron holes, than the appropriate ratio  $N_n/N_p$  might result from including excitations from the  $f, p$ , and  $i_{13/2}$  subshells for neutrons and only the  $s$  and  $d$  subshells for protons [48]. This could give a ratio  $N_n/N_p \geq 2$ , instead of 1.5. Since both odd and even parity unoccupied levels are present above neutron and proton shell gaps, either even or odd parity excitations could occur this way.

We find that the ratio  $M_n/M_p$  is 2.9 for the  $2_1^+$  level of  $^{206}\text{Pb}$ , but 2.1 for that of  $^{204}\text{Pb}$ . For both  $3_1^-$  levels we find ratios of about 1.9. Thus, not surprisingly, none of these low-lying levels are quite isoscalar, but as one moves away from doubly closed  $^{208}\text{Pb}$ , the even parity excitations seem to move toward being isoscalar.

RPA calculations using a separable interaction and including pairing have been done for collective excitations of these nuclei [49], which provide an expected ratio of 2.2 for the  $2_1^+$  levels of  $^{204,206}\text{Pb}$ . Our results suggest a rather larger ratio for  $^{206}\text{Pb}$ , but essentially the RPA expectation for  $^{204}\text{Pb}$ . The RPA results for the  $3_1^-$  excitations suggest ratios close to  $N/Z$ , whereas we find numbers a little larger than that, showing some neutron dominance even in those levels.

The inelastic neutron scattering cross sections for the  $3_1^-$  level of  $^{208}\text{Pb}$  measured by Annand *et al.* [19] and re-analyzed by Cheema and Finlay [47] projected a value of the  $E3$  coupling strength which, when compared to EM results [14], also suggests a ratio  $M_n/M_p$  of about 1.9 for the  $3_1^-$  level of that nucleus. Thus the octupole strengths are the same for all three nuclei either in neutron scat-

tering or in EM excitation, but the neutron scattering amplitudes are 27% stronger than the EM amplitudes.

### V. SOM MODEL vs CC DISPERSION CORRECTIONS

Dispersion corrections to the real scattering potential arise from the energy dependence of the imaginary potentials [20]. One very important power of these corrections is that they connect the real part of the scattering potential to that needed to properly bind single particle and single hole levels. A thorough analysis of the potential modifications wrought by dispersion corrections had been developed by C. H. Johnson *et al.* [18] for neutron scattering from  $^{208}\text{Pb}$ . The analysis used results spanning the energy region from the Fermi energy,  $-6$  MeV, or midway between occupied and unoccupied bound states, to 165 MeV.

To make such corrections for our scattering potentials we needed absorptive or imaginary potential information at energies well beyond the range of this experiment. The energy dependence of the absorptive potentials above 8 MeV and the Fermi energy were taken from the analysis of Johnson *et al.* [18]. The Fermi energy and the Hartree-Fock potential which served as the base of the scattering field of that work [18] are just the ones needed here, since we deal with the same single particle and hole states. We found, in the course of analysis, that raising the radius of that potential by 0.01 fm allowed the potential strengths generated with the Hartree-Fock potential and the dispersion corrections to match very well the strengths we needed to describe our scattering results at all energies.

One problem with the results of these methods, which have usually employed spherical potential models near magic nuclei [18,21], is that although they do well with the bound state region and the high energy scattering region, they have not represented well the scattering strengths needed at low neutron energies, from 2 to 8 MeV. Jeukenne, Johnson, and Mahaux argued [50] that this could reflect highly energy-dependent absorption effects, owing to the onset of strong inelastic collective effects. There was even a suggestion that angular momentum dependent absorption would obtain, owing to the specific multipolarity of inelastic collective excitations [50]. The dispersion corrections these authors made for  $^{208}\text{Pb}$  and many previous dispersion corrections were developed within the SOM description of scattering, in which collective excitations are treated only implicitly, as part of the overall absorption.

Dispersion corrections, however, had been developed [22] for a CC description of the strong collective excitations in the Os and Pt isotopes, using CC methods to describe the scattering, including explicitly both  $2_1^+$  and  $3_1^-$  collective excitations. The shape-transitional Os and Pt isotopes are highly susceptible to electric quadrupole excitations, and for the tests completed [22] three members of the ground-state quadrupole band, the band-head of the gamma band, and the  $3^-$  excitations were explicitly coupled into the scattering description. The CC scattering model, with dispersion corrections, provided good

descriptions of scattering strength for bound-state energies, low-energy scattering, and medium-energy scattering. At the same time, no SOM could be found to successfully describe scattering from these highly collective nuclei, even with dispersion corrections. The low-energy problem which had plagued the spherical models for  $^{208}\text{Pb}$  was not present for these CC models in Os and Pt. It was considered possible that explicit inclusion of strong coupling to the most important collective excitations would resolve the problem of low-energy scattering strengths in analyses for magic and semimagic nuclei, as well.

The presently studied Pb nuclei offer an excellent opportunity to further test comparisons between dispersion-corrected SOM and CC models. We have constructed both spherical and CC descriptions of our scattering data in these Pb isotopes. One can see, however, in Tables II and III that the SOM and CC potentials are very little different for these nuclei; primarily the CC surface absorptive potential is somewhat weaker than that of the SOM, though other parameters are also slightly affected. The energy dependencies of the CC and SOM absorptive potentials are similar enough that the dispersion corrections for the two models are quite similar.

Dispersion corrections were calculated for both the spherical model and CC model using the methods described earlier. [22] The results for the dispersion corrections are shown in Fig. 10; all values are plotted as volume-integrals per nucleon ( $J_R/A$ ) of real potential components. The dot-dashed curve is the surface correction ( $\Delta J_D/A$ ), derived from the surface absorption potential; this correction is similar for either the spherical or coupled-channels model. The dotted curve is the volume absorption correction ( $\Delta J_V/A$ ), which is the same for both models, since it is taken from the volume absorptive potential of Ref. [18]. The volume-integral per nucleon of the Hartree-Fock (HF) type potential,  $J_{\text{HF}}/A$ , is shown as the dashed line, with its normal linearly decreasing energy dependence. The HF potential used was that of Ref. [18] except for the noted slight increase of 0.01 fm in the radius. The sum of the surface and volume correction terms along with the HF term is given by the solid curve

$$J_R/A = (J_{\text{HF}} + \Delta J_V + \Delta J_D)/A .$$

All curves drawn were from the CC model analyses. However, little difference is seen in the SOM. The data points in Fig. 10 are from our CC analyses and are to be compared to the dispersion corrected strengths shown as the solid curve. Except for the point at 8 MeV, the agreement with the strengths expected from a proper dispersion corrected potential is quite good. The values of  $J_R/A$  needed for the fits at the three energies using the SOM are well within uncertainties the same as those plotted in Fig. 10 for the CC analyses.

The dispersion corrections calculated for scattering from  $^{204}\text{Pb}$  for the SOM and CC models give very similar corrections. They show results very similar to those shown in Fig. 10 for  $^{206}\text{Pb}$ . Thus both models provide good representations of potential strengths needed to fit scattering cross sections at the three incident energies of

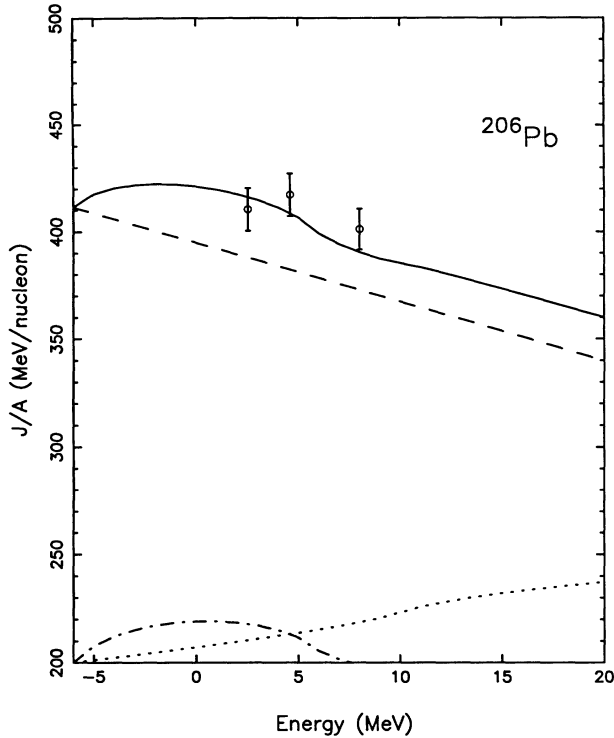


FIG. 10. Volume integral of the real potential strength per nucleon. The Hartree-Fock term,  $J_{\text{HF}}/A$ , is shown by the dashed line, with the normal linear decrease with increasing energy. The correction term from the surface absorptive potential,  $J_D/A$ , is shown by the dash-dotted curve near the bottom of the panel. The volume absorption correction,  $J_V/A$  is shown by the dotted curve. The solid curve is the sum of all terms, representing the full energy-dependent mean field. The open points are potential strengths needed to represent total and differential elastic scattering cross sections at the indicated energies; one sees that the corrected strengths are well represented by the mean scattering field. The correction terms themselves shown at the bottom of the figure each have 200 added to them, to keep the figure compact.

this experiment for both nuclei. We find, in fact, that for either the SOM or the FOV model that we are able to include the bound states and the scattering continuum, most notably the energy region between 2 and 8 MeV, in our overall description. At least in these nuclei, where only the first  $2^+$  and first  $3^-$  levels are appreciably excited, and where the first-order vibrational model is all that is needed, directly coupling those two excitations into the model space affects the scattering description very little, except for cross sections to those two excited levels themselves.

The generally good correspondence of SOM and CC dispersion analyses for scattering from these Pb nuclei differs markedly from the results for strongly collective nuclei [22], and also from the results for scattering from the less strongly collective and semimagic even- $A$  Sn nuclei [51]. Dispersion correction tests for both sets of nuclei show marked differences between results for CC and SOM

TABLE IV. Ratios of target neutron amplitudes to target proton amplitudes,  $M_n/M_p$ , for participation in particular collective excitations, as inferred from neutron scattering combined with electromagnetic excitation, and also from  $^{17}\text{O}$  scattering combined with Coulomb excitation. If all nucleons participate equally, the ratio should be  $N/Z$ , which is about 1.5

	$M_n/M_p$ - $n$ scattering		$M_n/M_p$ - HI scattering <sup>a</sup>	
	$2_1^+$	$3_1^-$	$2_1^+$	$3_1^-$
$^{206}\text{Pb}$	$2.9 \pm 0.1$	$1.93 \pm 0.1$	2.5 - 3.0	$\simeq 1$
$^{204}\text{Pb}$	$2.1 \pm 0.1$	$1.91 \pm 0.1$	2.1	$\simeq 1$

<sup>a</sup>Reference [15].

models. In fact, SOM models cannot represent scattering and bound states; CC models alone suffice. This was not so surprising for the strongly collective nuclei, but is more surprising for Sn nuclei, since FOV models such as that used in this work also are approximately adequate for them. Actually the direct coupling to  $2^+$  and  $3^-$  levels in Sn have amplitudes 1.5 to 3 times as large respectively as those for these Pb nuclei; that may be the reason SOM and CC models provide nearly indistinguishable mean fields for Pb, but very different for the Sn nuclei.

## VI. CONCLUSIONS

These neutron scattering cross sections have been analyzed with both spherical and CC models. We find that the energy dependence of the mean scattering field is consistent with results using a dispersion relation which connects the real and imaginary parts of the scattering potential. The ratios  $M_n/M_p$  for electric quadrupole excitations, the  $2_1^+$  levels for both  $^{204,206}\text{Pb}$  have been extracted from the neutron scattering data and are found to be more than 90% for  $^{206}\text{Pb}$  and 45% for  $^{204}\text{Pb}$  stronger than would be implied by isoscalar excitations. The octupole coupling amplitudes observed in neutron scattering from  $^{204,206}\text{Pb}$  have almost the same strength as seen in neutron scattering from  $^{208}\text{Pb}$  at similar incident energies. That  $E3$  coupling strengths from  $^{208}\text{Pb}$  to  $^{204}\text{Pb}$  are nearly constant is consistent with the constancy observed for EM excitation strengths. However, all of these neutron strengths are about 28% stronger than would be implied by isoscalar excitations.

The enhanced role of target neutrons in the first  $2^+$  levels is very similar to enhancements reported from heavy-ion scattering, as shown in Table IV, and from comparisons of  $\pi^+$  to  $\pi^-$  scattering. This work does report weak neutron dominance for the low-lying  $E3$  excitations, whereas the heavy-ion and pion scattering experiments suggest approximate equality of neutron and proton roles. Detailed examination of all three experiments suggest, however, that this difference could be the result of enhanced sensitivity in the present experiment with nucleons.

## ACKNOWLEDGMENTS

The support of the National Science Foundation for this project through Grants PHY-8702369, PHY-

9001465, and PHY-9002860 is gratefully acknowledged. We acknowledge with appreciation discussions with C. H. Johnson of Oak Ridge National Laboratory, C. Mahaux of Liege, Belgium, and Jesse L. Weil of the University of Kentucky.

- [1] S. E. Hicks, J. P. Delaroche, M. C. Mirzaa, J. Hanly, and M. T. McEllistrem, *Phys. Rev. C* **36**, 73 (1987).
- [2] S. E. Hicks, Z. Cao, M. C. Mirzaa, J. L. Weil, J. M. Hanly, J. Sa, and M. T. McEllistrem, *Phys. Rev. C* **40**, 2509 (1989).
- [3] T. B. Clegg, G. Haouat, J. P. Delaroche, Ch. Lagrange, J. Chardine, S. E. Hicks, G. R. Shen, and M. T. McEllistrem, *Phys. Rev. C* **40**, 2527 (1989).
- [4] M. T. McEllistrem, in *Proceedings of the International Conference on High Spin Physics and Gamma-Soft Nuclei*, edited by R. A. Sorenson and J. X. Saladin (Pittsburgh/Carnegie Mellon University, Pittsburgh, 1990).
- [5] R. S. Mackintosh, *Nucl. Phys.* **A266**, 379 (1976).
- [6] Joseph N. Ginocchio and Amiram Leviatan, *Ann. Phys. (N.Y.)* **216**, 152 (1992).
- [7] Ch. Lagrange, J. Lachkar, G. Haouat, R. E. Shamu, and M. T. McEllistrem, *Nucl. Phys.* **A345**, 193 (1980).
- [8] A. M. Bernstein, V. R. Brown, and V. A. Madsen, *Comments Nucl. Part. Phys.* **11**, 203 (1983), and references cited therein.
- [9] M. A. Kennedy, P. D. Cottle, and K. W. Kemper, *Phys. Rev. C* **46**, 1811 (1992).
- [10] D. Wang and M. T. McEllistrem, *Phys. Rev. C* **42**, 252 (1990).
- [11] J. M. Hanly, S. E. Hicks, S. W. Yates, and M. T. McEllistrem, *Phys. Rev. C* **37**, 1840 (1988).
- [12] P. W. F. Alons, H. P. Blok, J. F. A. Van Hienen, J. Blok, *Nucl. Phys.* **A367**, 41 (1981).
- [13] P. D. Cottle, K. A. Stuckey, K. W. Kemper, *Phys. Rev. C* **38**, 365 (1988).
- [14] R. H. Spear, *At. Data Nucl. Data Tables* **42**, 55 (1989).
- [15] D. J. Horen, R. L. Auble, F. E. Bertrand, M. L. Halbert, G. R. Satchler, M. Theonnessen, R. L. Varner, V. R. Brown, P. L. Anthony, and V. A. Madsen, *Phys. Rev. C* **44**, 128 (1991).
- [16] D. J. Horen, C. L. Morris, S. J. Seestrom, F. W. Hersman, J. R. Calarco, M. Holtrop, M. Leuschner, Mohine Rawool-Sullivan, R. W. Garnett, S. J. Greene, M. A. Plum, and J. D. Zumbro, *Phys. Rev. C* **46**, 499 (1992).
- [17] Sally F. Hicks, S. E. Hicks, G. R. Shen, and M. T. McEllistrem, *Phys. Rev. C* **40**, 2560 (1990).
- [18] C. H. Johnson, D. J. Horen, and C. Mahaux, *Phys. Rev. C* **36**, 2252 (1987).
- [19] J. R. M. Annand and R. W. Finlay, *Nucl. Phys.* **A443**, 249 (1985).
- [20] C. Mahaux and H. Ngo, *Phys. Lett.* **100B**, 285 (1981).
- [21] C. Mahaux, H. Ngo, and G. R. Satchler, *Nucl. Phys.* **A449**, 354 (1986); C. Mahaux and R. Sartor, *Phys. Rev. Lett.* **57**, 3015 (1986); C. Mahaux and R. Sartor, *Nucl. Phys.* **A458**, 25 (1986).
- [22] S. E. Hicks and M. T. McEllistrem, *Phys. Rev. C* **37**, 1787 (1988).
- [23] John M. Hanly, Ph. D. dissertation, University of Kentucky, 1987.
- [24] Steven E. Hicks, Ph. D. dissertation, University of Kentucky, 1987.
- [25] F. H. Frohner, AEC Research and Development Report Number GA-8380, 1968.
- [26] Z. Zhou, J. L. Weil, and R. L. Winters, *Bull. Am. Phys. Soc.* **30**, 1252 (1985).
- [27] A. Smith, R. Holt, and J. Whalen, Argonne National Laboratory Report ANL/NDM-43, 1978 (unpublished); R. Schwartz, R. Schrack, and D. Heaton, in *Neutron Scattering from  $^{12}\text{C}$  in the few-MeV Region*, Natl. Bur. Stand. Pub. No. NBS-138 (U.S. GPO, Washington, DC, 1974).
- [28] Pb totals from 3 MeV to 8 MeV, measured at ORELA.
- [29] M. C. Mirzaa, J. P. Delaroche, J. L. Weil, J. Hanly, and M. T. McEllistrem, *Phys. Rev. C* **32**, 1488 (1985).
- [30] John R. Lilley, "MULCAT-BRC, A Monte Carlo Neutron and Gamma-Ray Multiple Scattering Correction," Internal Service de Physique et Techniques Nucléaires, Centre d'Études de Bruyères-le-Châtel, Report P2N/934/80, 1980.
- [31] D. E. Velkley, D. W. Glasgow, J. D. Brandenberger, and M. T. McEllistrem, *Nucl. Instrum. Methods* **129**, 231 (1975).
- [32] W. Galati, J. D. Brandenberger, and J. L. Weil, *Phys. Rev. C* **5**, 1508 (1972).
- [33] L. Stewart, R. J. LaBauve, P. G. Young, Los Alamos National Laboratory Report LA-4574, ENDF-141, 1991.
- [34] G. Haouat, J. Lachkar, J. Sigaud, and Y. Patin, Service de Physique et Techniques Nucléaires, Centre d'Études de Bruyères-le-Châtel, Report CEA-N-2080, 1979.
- [35] D. J. Horen, J. A. Harvey, and N. W. Hill, *Phys. Rev. C* **18**, 722 (1978).
- [36] J. A. Farrell, G. C. Kyker Jr., E. G. Bilpuch, and H. W. Newson, NNDC tabulations, Brookhaven National Laboratory, 1961.
- [37] J. L. Fowler and E. C. Campbell, NNDC tabulations, Brookhaven National Laboratory, 1962.
- [38] Dale W. Glasgow and D. Graham Foster, Jr., *Phys. Rev. C* **3**, 604 (1971).
- [39] Y. Tomita, S. Tanaka, and M. Maruyama, Report No. Jaeri-M-5418, 1973.
- [40] G. Haouat, J. Sigaud, J. Lachkar, Ch. Lagrange, and Y. Patin, International Atomic Energy Agency Report No. NEANDC(E)-180, 1978; G. Haouat, J. Lachkar, Ch. Lagrange, J. Jary, and Y. Patin, *Nucl. Sci. Eng.* **81**, 491 (1982).
- [41] T. Tamura, *Rev. Mod. Phys.* **37**, 679 (1965).
- [42] J. R. M. Annand, Ohio University report, 1984 (unpublished; available from R. W. Finlay, Physics Department).
- [43] H. M. Hofmann, J. R. Richert, and J. W. Tepel, *Ann. Phys. (NY)* **90**, 391 (1975); **90**, 403 (1975); J. W. Tepel, H. M. Hofmann, and M. Herman in *Nuclear Cross Sections for Technology*, Proceedings of the International Conference, edited by J. L. Fowler, C. H. Johnson, and C. D. Bowman, Natl. Bur. Stand. Spec. Pub. No. 594 (U.S. GPO, Washington, DC, 1979), p. 762.
- [44] M. T. McEllistrem, in *Proceedings of the International*

- Conference on Neutron-Nucleus Collisions, A Probe of Nuclear Structure*, edited by J. Rapaport, R. W. Finlay, S. M. Grimes, and F. S. Dietrich, AIP Conf. Proc. No. 124 (AIP, New York, 1985), p. 208.
- [45] J. Raynal, Report No. ECIS79 (unpublished); J. Raynal, *Computing as a Language of Physics* (IAEA, Vienna, 1972); *The Structure of Nuclei* (IAEA, Vienna, 1972), p. 75; J. Raynal, Phys. Rev. C **23**, 2571 (1981).
- [46] S. Raman, C. H. Malarkey, W. T. Milner, C. W. Nestor, Jr., and P. H. Stelson, At. Data Nucl. Data Tables **36**, 1 (1987).
- [47] T. S. Cheema and R. W. Finlay, Phys. Rev. C **37**, 910 (1988).
- [48] Aage Bohr and Ben R. Mottelson, *Nuclear Structure* (Benjamin, New York, 1969), Vol. I, p. 324 ff.
- [49] V. R. Brown, J. A. Carr, V. A. Madsen, and F. Petrovich, Phys. Rev. C **37**, 1537 (1988).
- [50] J.-P. Jeukenne, C. H. Johnson, and C. Mahaux, Phys. Rev. C **38**, 2573 (1988).
- [51] M. Mirzaa, R. Harper, M. T. McEllistrem, Z. Zhou, A. A. Naqvi, and J. L. Weil, Phys. Rev. C (submitted).